



DELPHI 86-65 CAL-38

18th June, 1986

A LOW-NOISE AMPLIFICATION CHAIN FOR THE
VACUUM PHOTO-TRIODE READ-OUT OF THE DELPHI LEAD GLASS CALORIMETER

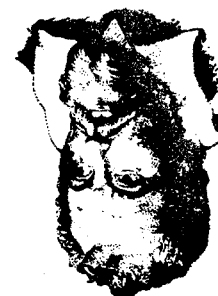
G.Barichello, M.Mazzucato, M.Pegoraro,
G.Zumerle

A LOW-NOISE AMPLIFICATION CHAIN
FOR THE VACUUM PHOTO-TRIODE
READ-OUT OF THE DELPHI LEAD
GLASS CALORIMETER.

G. Barichello, M. Mazzuccato, M. Pegoraro and
G. Zumerele

I.N.E.N.-ISTITUTO NAZIONALE DI FISICA NUCLEARE
SEZIONE DI PADOVA

UNIVERSITÀ DEGLI STUDI DI PADOVA
DIPARTIMENTO DI FISICA "GALILEO GALILEI"



In this paper we describe the low noise electronic amplification chain for the vacuum photo-triode read-out of the DELPHI lead glass calorimeter of the final experiment. A mean open input noise of 166 e_{RMS} has been obtained with unipolar shaping. For completeely mounted photo-triodes in a situation very close to the final experimental set-up and bipolar shaping we get a mean noise of 292 e_{RMS}. Complete immunity against 1/f noise has been obtain ed. The gain stability during six months of operation is better than 40.3%.

Abstract

A. Bartolucci, M. Mazzucato, M. Pegoraro, G. Zumerle
Istituto Nazionale di Fisica Nucleare, Sezione di Padova
OF THE DELPHI LEAD GLASS CALORIMETER
A LOW-NOISE AMPLIFICATION CHAIN FOR THE VACUUM PHOTOTRIODE READ-OUT

Introduction

In the End-Cap electromagnetic calorimeter of the DELPHI experiment (FEMC) (1), based on Lead Glass counters, newly developed one-stage photo-multipliers ("photo-triodes", (2)) have replaced the popular multistage tubes because they can operate in a high magnetic field. It is important not to spoil the precision offered by Lead Glass counters and since the mean charge from such photo-triodes is in the EC range, high gain electronic amplification with very low noise is required in order to match the input ranges of commercially available analog to digital converters (ADC's). For the 10000 channels of FEMC we have developed a special front-end to obtain a resolution and a dynamic range capability of 12 bits at a price significantly lower than currently available commercial products.

In this paper we will describe the performance of the analog part of such an electronic chain which includes the charge preamplifier, the filter and the track and converter, the latter being converted analog to digital hold off the charge for the multilevel analog to digital conversion. This part is now available in the form of two hybrids at a total cost of about 60 SFM. In hyperids, the input charge is dependent on $h(t)$, where t is the time constant of the detector. The output of the detector is given by the general expression (3)

The photo-triodes consist of a photodiode, one diode and an anode as shown in Fig. 1. The photo-triodes use is determined by the distances between the electrodes which vary from one manufacturer to another. Typically measured values range from 5 to 15 pF. The triode gain in a magnetic field of 1.0 Tesla is in the range 7±10. An e.m. shower which develops in SF1 lead glass generates ~1000 photoelectrons/GeV on a bialkali triode photodiode. This

noise ratio, in the presence of series and parallel noise, the best signal to noise ratio is obtained when R_s and R_p are the equivalent noise generators that account for the series and parallel noise contributions of the whole amplification chain, see Fig. 3, and C_i is the total (detector+PMT+test+parasitic) input capacitance. It is well known (3) that to obtain the best signal to noise ratio, in the presence of series and parallel noise generators that account for the series and parallel noise contributions of the whole amplification chain, see Fig. 3, and C_i is the total (detector+PMT+test+parasitic) input capacitance. The input current is given by the equation

$$(1) \quad ENC^2 = \frac{2KT}{R_p} \int_{-\infty}^{\infty} [h(t)]^2 dt + 2KT R_s C_i^2 \int_{-\infty}^{\infty} [h'(t)]^2 dt .$$

The overall linear chain is shown in Fig. 2. It consists of a preamplifier, located close to the triode to minimize the connecting lead length, connected to a time-invariant filter through 50 m of twisted pair cable. The overall chain has a response such that the maximum of the output pulse is proportional to the integrated charge. For a $a_0(t)$ input charge the output is $h(t)$. The equivalent noise is given by the general expression (3)

Charge Amplification

The dynamic range is of the order of 4000. The integrated charge (ENC) must be kept to around 25 e-. To keep a good energy and position resolution the counter noise has to be around 25 MeV hence the equivalent noise charge (ENC) has to be around 25 e-. In the LEP accelerator is 22 ns which allows one to use large shaping time constants.

$$Q_M = 8 \cdot 10^5 \text{ e}^- .$$

determines the maximum collected charge and we have assumed for the final design:

In the control room the signals are fed into the shaping amplifier cards containing in the prototype versions 16 or 24 channels. The schematics of the filter amplifier is shown in Fig. 5. The jumper j_1, j_2 allows the choice between unipolar and bipolar shaping. The first waveform in principle optimizes the noise performance of the chain and is limited to low-counting rates. The second one allows higher counting rates, very useful when calibrating the detector with an electron beam, and has a much higher resolution of 3000 Hz.

The first stage of the filter consists of a differential receiver performing a first integration with a time constant of 0.5 μ s. This assures good common mode rejection against interference such as external pick-up noise, cross talk between channels and ground loops.

After this stage there is a pole-zero circuit with time constant 1.5 μ s to perform a suitable shaping.

The final amplification stage for the unipolar shaping jumper inserted) consists of an approximate integration to obtain the final waveform. The bipolar pulse is obtained by further approximation through the three 300PF capacitors that increases the rejection of low frequency noise by

The AC coupling between anode and preamplifier, although it increases the noise slightly, is introduced to avoid a shift of the working point of the preamplifier, which would originate, through R_f , from the dark current of the tube. The diode protects the input FET against the negative spikes that can occur when the HV for the triode is switched on/off. Since it injects noise directly into the preamplifier, it has been chosen to have small inverse currents (50 pA typical) and small capacitance $C_{\text{di}} = 1 \text{ pF}$. The power dissipation of this preamplifier, determined essentially by the output stage, is about 300 mW.

Final Amplification

The LRF beam crossing interval allows one to reach a statistical approximation to these conditions without using too complex circuitry. Our solution is a double integration with optimum delay one or two differentiations to implement unipolar or bipolar shaping.

$$(2) \quad ENC_2^{opt} = 4KT C_1 \sqrt{\frac{R}{s}} \cdot$$

is the noise corner time constant. In these conditions the parallel and series noise contributions are equal and the ENC reaches a minimum. This is a general behavior which it is independent of the precise shape of the pulse response. It is also known that the minimum ENC is obtained for the ideal cusped waveform (3) and is given by

We have adopted a JFET preamplifier in a charge sensitive configuration. The circuit is shown in Fig. 4 to - gether with the HV polarization circuit for the tritode. The preamplifier, originally developed for μ-strip silicon detectors with the HV polarization circuit shown in Fig. 4 to - is commerically available as a single channel hybrid (5).

In the charge sensitive loop, the AC feedback applied by C_F provides the charge integration while DC feedback via R_F allows the capacitance discharge with time constant $R_C F$. For good noise performance R_F should be as high as possible. The open input R_p^d is, in fact, given by R_F in parallel with the FET parallel equivalent resistance R_F^d in practice. R_F^d is limited to 100 MΩ which is a value current - ly attainable with hybrid techniques.

The second stage is a pole-zero cancellation that reduces the signal length from 100 ns to 10 ns. This avoids pile-up effects in the output stage as well as amplification of the low frequencies. The gain which is determined by the ratio R_c^d is chosen to give differential outputs of 90+90 mV for the maximum signal O_m .

The charge sensitive integrative loop, the AC feedback applied by C_f provides the charge integration which DC feedback via R_C . For good noise performance R_f should be as high as possible. The open input R_p is, in fact, given by R_f in parallel with the FET parallel equivalent resistance $R_{A10/g}$. In practice R_p is limited to 100 MΩ which is a value current-attainable with hybrid techniques.

The second stage is a pole-zero cancellation that reduces the signal length from 100 ns to 10 ns. This avoids diode-up effects in the output stage as well as amplification of the low frequencies. The gain which is determined by the ratio R_b/R_a is chosen to give differential outputs of 90+90 mV for the maximum signal O_m .

The final output buffer allows a symmetrical driving for the maximum signal Q_m . The ratio $\frac{R}{L}$ is chosen to give differential outputs of $90+90$ mV at the low frequencies. The gain which is determined by the feedback elements in the output stage as well as amplification of the feed-back errors from 100 ns to 10 ns. This avoids distortion of the signal levels from 100 ns to 10 ns.

The second stage is a pole-zero cancellation that reduces the second lenth from 100 ns to 10 ns. This avoids pile-up effects in the output stage as well as amplification of the low frequencies. The gain which is determined by the ratio R_c/R_b is chosen to give differential outputs of $90+90 \text{ mV}$ for the maximum signal O_m . The final output buffer allows a symmetrical driving

The final output buffer allows a symmetrical driving for the maximum signal Q_m .

The theoretical estimation of the noise using expression (1) depends on the FET transconductance. Using a mean value $G_m = 10 \text{ mA/V}$ which gives $R_s = 69 \Omega$, we obtain for unipolar noise $\text{EN}_{\text{G}} = (270 \pm 20) \text{ e}^-$.

- (a) the triode dark current ($I_{SD} = 1 \text{ nA}$)
 - (b) the triode input capacitance ($C_{AK} = 5 \text{ pF}; C_{AD} = 10 \text{ pF}$)
 - (c) the AC anode coupling
 - (d) the diode reverse current and capacitance.
- Individual bench measurements, made on a sample of about 50 completely mounted triodes, with bipolar shaping, give

The most important are:
increases due to the contributions from additional noise sources.
When the triodes are connected as in Fig. 4 the ENC increases one. It peaks at $1.25 \mu\text{s}$.

These values do not change when one varies the overall gain in the range $1 \text{ to } 20 \text{ MV/e}^-$.

$\text{EN}_{\text{G}} = (204 \pm 9) \text{ e}^-$.
With bipolar shaping the same measurements give

$\text{EN}_{\text{G}} = (166 \pm 9) \text{ e}^-$
The mean open input ENC and RMS spread for about 20 unselected hybrids is
value of $2.2 \text{ e}^-/\text{pF}$ and tends asymptotically to $6.0 \text{ e}^-/\text{pF}$.
with the input shunt capacitance; the slope has a starting runction of the detector capacitance. The noise increases FET's such as the MBF4393 or BSRS58 is given in Fig. 7 as a FET noise ENC, using the unipolar shaping, typical of

Noise Results

For easy noise measurements a wideband RMS voltmeter HP 3400A has also been used.
In no case did one observe an appreciable difference in performance which might depend on the technique adopted.

The results were summarized here come from bench tests on single channels and from a series of measurements performed on a calorimeter module designed to contain 96 ref. (6), was in operation in the DELPHI test beam H6 counters. This module, similar to the one described in ref. (6), was in operation in the DELPHI test beam H6 at the CERN North Hall from May to December 1985.
The unipolar and bipolar impulse response of the electron-positron chain to a square calibrated pulse, injected on the input test capacitance (1 pF), are shown in Figs 6a and 6b respectively.
The unipolar shaping has the following typical characteristics:
- peak at $2.12 \mu\text{s}$
- ratio $h(20 \mu\text{s})/h(2.12 \mu\text{s}) = 0.9 \times 10^{-4}$
- charge gain: 2.25 MV/e^- .
The bipolar pulse is the approximate derivative of the previous one. It peaks at $1.25 \mu\text{s}$.

The noise measurements of the output signals were made under various experimental conditions with the different techniques summarized below.
The measurements of the output signals were made under various sense mode,
(a) using a multichannel analyzer Selenia 7412 operated in peak sense mode,
(b) via a Leccroy 2282 12 bit charge sensitive ADC sensing through a resistor the hold voltage of the shaper with a 1 μs gate
(c) using the 50 Ω amplifier driver stage, shown in Fig. 5, as an alternative to the track-and-hold circuit, to feed the shaper output of Fig. 6 directly into the Leccroy ADC. The peak was measured synchronizing a 70 ns gate with the broad signal maximum.

The final stage is a track-and-hold circuit designed to keep the charge for at least 500 μs with a loss smaller than one least count. During this time we intend to multiply the charge to 12 bit analog to digital conversion of about 100 channels.

Performance

about 40 dB.

We are now developing the final version of the cards in FASTBUS format. Each card will serve 80 channels and will provide the amplification, the track-and-hold, the

The performance of the electronic chain to be used in the Lead Glass e.m. calorimeter of the DELPHI experiment satisfies the tight constraints imposed by the required detector performance. The bipolar shaping gives an ENC=270e RMS. The system is linear to better than 0.5% up

Conclusions

Fig. 10 shows the distribution of the electronic sensitivity, obtained by sending a calibrated pulse into the test-input capacitances. The width is compatible with the tolerance (20%) of such components.

The system stability has been checked over a period of six months. The pedestal value of a typical channel is shown in Fig. 11 as a function of runnning time. All the channels are stable within 2 ADC counts.

The sensitivity of a typical channel measured through the responses to a calibrated pulse into the test input capacitance is shown in Fig. 12 as a function of the running time. The amplitude is stable at the $\pm 0.3\%$ level.

Thus value is also comparable within 10% with the results of the remaining 22 photo-triodes made by different manufacturers or with different construction technique.

$\langle ENC \rangle = (292 \pm 26) \text{ eV}$

The signals from the preamplifiers, located inside the module, were sent through 50 meter cables, each consisting of 16 twisted pairs, to the cards performing the amplitude discrimination, 16 bipolar filterbanking, and the track-and-hold. The outputs of these cards were then digitized by 2282 Lecroy ADC's and read out via a VAX750 computer. The mean ENC obtained in these conditions, which are very similar to those of DELPHI, is, for the 50 photo-trig

A module consisting 72 counters, equipped with the electronics described above, has been in operation since June 1985. The same HV (800 V) was applied to all the tridodes.

This assures 12 bit accuracy over a conversion time of at least 500 μs.

- drop rate: 0.1 volt/sec
 - charge injection: 3.5 pc
 - feed-through less than 0.025%.

The main measured characteristics are:

The dynamic range capability of the electroacoustic chain is given in Fig. 9. The integral linearity is better than 0.5% over the whole dynamic range.

DYNAMIC RANGE AND LINEARITY

values in the range 1-3 KHz. The exact values and the amplitude of the effect depend on the photo-triode type. In the presence of acoustic noise at resonance frequencies, therefore, the ENC for unipolar snapping increases with the applied HV. This behavior is shown in Fig. 8, where the noise dependence on the applied HV is shown for different conditions. The bipolar shaping circuitry filters out the low frequency part of the signal, so that the noise is not affected by the presence of acoustic vibrations.

The system is in principle sensitive to mechanical vibrations that can cause oscillations of the bridge capacitance. This has been tested using a loud-speaker excited at varying frequencies. We observe a resonant behavior of the system noise for unipolar shaping at discrete frequency

and bipolar shaping $ENC=209e^-$ and $ENC=240e^-$ respectively - very close to the experimental value . With the optimal shaping given by expression (2) we would expect an $ENC_{opt}=169e^-$.

Multichanneler and the 12 bit ADC.

Acknowledgement

The authors are indebted to S. Centro and P.F. Mandelli for their advise and invaluable assistance in the design of this chain.

References

1. Delphi Progress Report CERN/LEPC 84/16,
2. M.D. Rousseau et al., IEE Trans. Nucl. Sci. Vol. NS30, 479, Feb. 83,
3. See P. Rehak, Enrico Fermi International School of Physics, Varenna, Lake Como, Italy, 1981 (3rd Course),
4. P.F. Manfredi: Electronics for silicon detectors in high energy experiments; Proceedings of the Meeting on Miniaturization of High Energy Physics Detectors, Pisa 1980;
5. The hybrid preamplifier is produced by AUREL, Trade name: LABEN, Milano; NEOM, Torino;
6. P. Checchia et al.: Study of a lead glass calorimeter with vacuum phototriode read-out, to be published in NIM.

Figure Captions

- Fig. 1. Construction of the Hamamatsu R2184 (type E) phototriode;
Fig. 2. Block diagram of the phototriode linear chain;
Fig. 3. Equivalent circuit of detector preamplifier and
filter for noise analysis;
Fig. 4. The photo-triode electrical connections and pre-
amplifier diagram;
Fig. 5. Filter amplifier and track-and-hold electrical diagram.
The circuit enclosed in the dotted rectangle
exists in hybrid form. The 50 Ω driving stage as an
alternative output is shown outside the dotted
rectangle;
Fig. 6. Analog chain response to an input charged of $2 \cdot 10^4$
electrons ($\text{Gain} = 15 \text{ UV/e}$);
Fig. 7. The noise ENC as a function of input capacitance;
Fig. 8. Noise ENC in the presence of resonant acoustic vibration
as a function of the applied HV;
Fig. 9. Dynamic range capability; the points represent the
deviation from the straight line fit to the
first half of the range. The sensitivity for this
measurement was 250 electrons/ADC count;
Fig. 10. Distribution of the electronic sensitivity of individual channels;
Fig. 11. Pedestal of a typical channel as a function of running time;
Fig. 12. Sensitivity of a typical channel as a function of running time.

Fig. 2

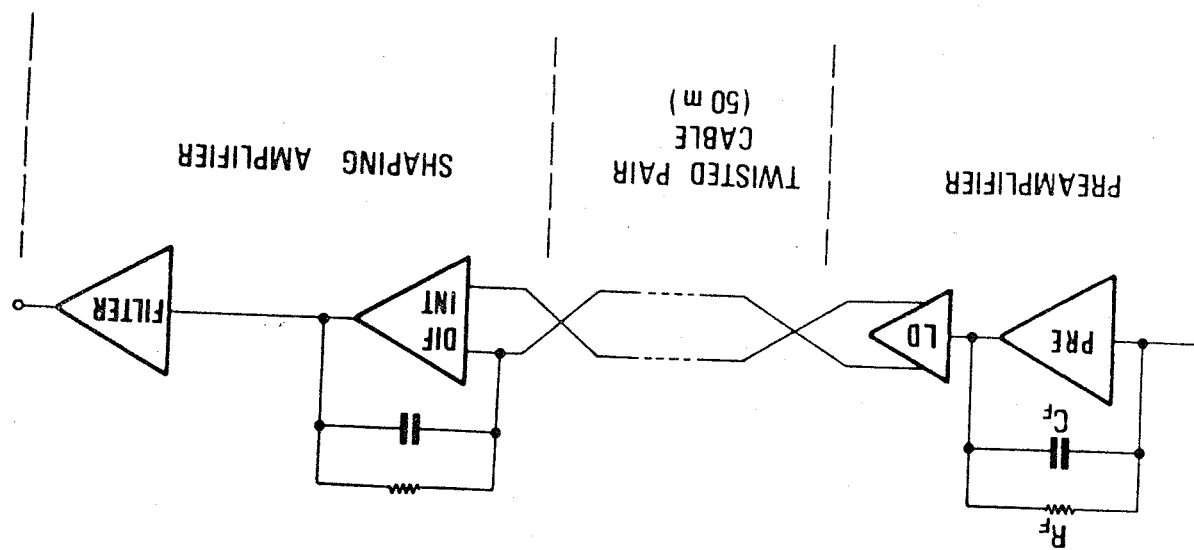
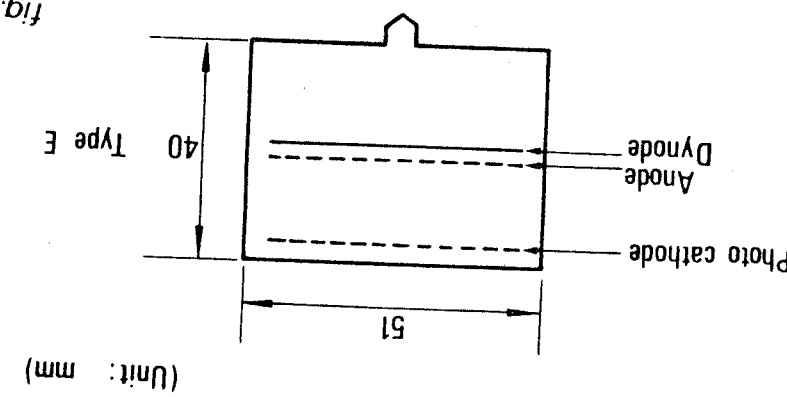


Fig. 1



TYPE R2184

fig. 4

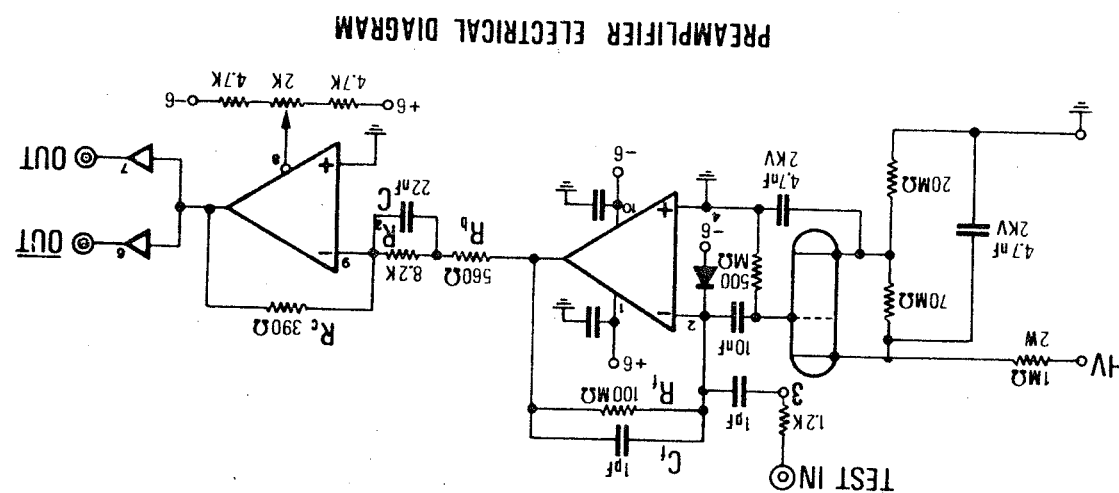


fig. 3

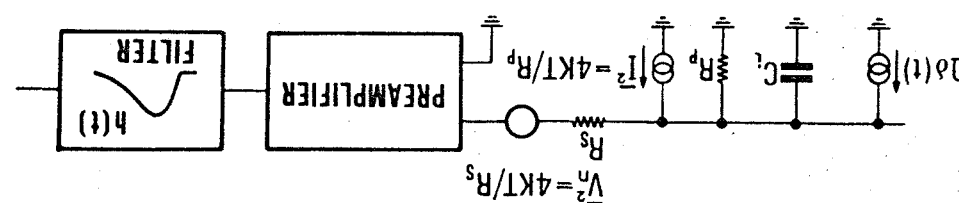


fig. 5

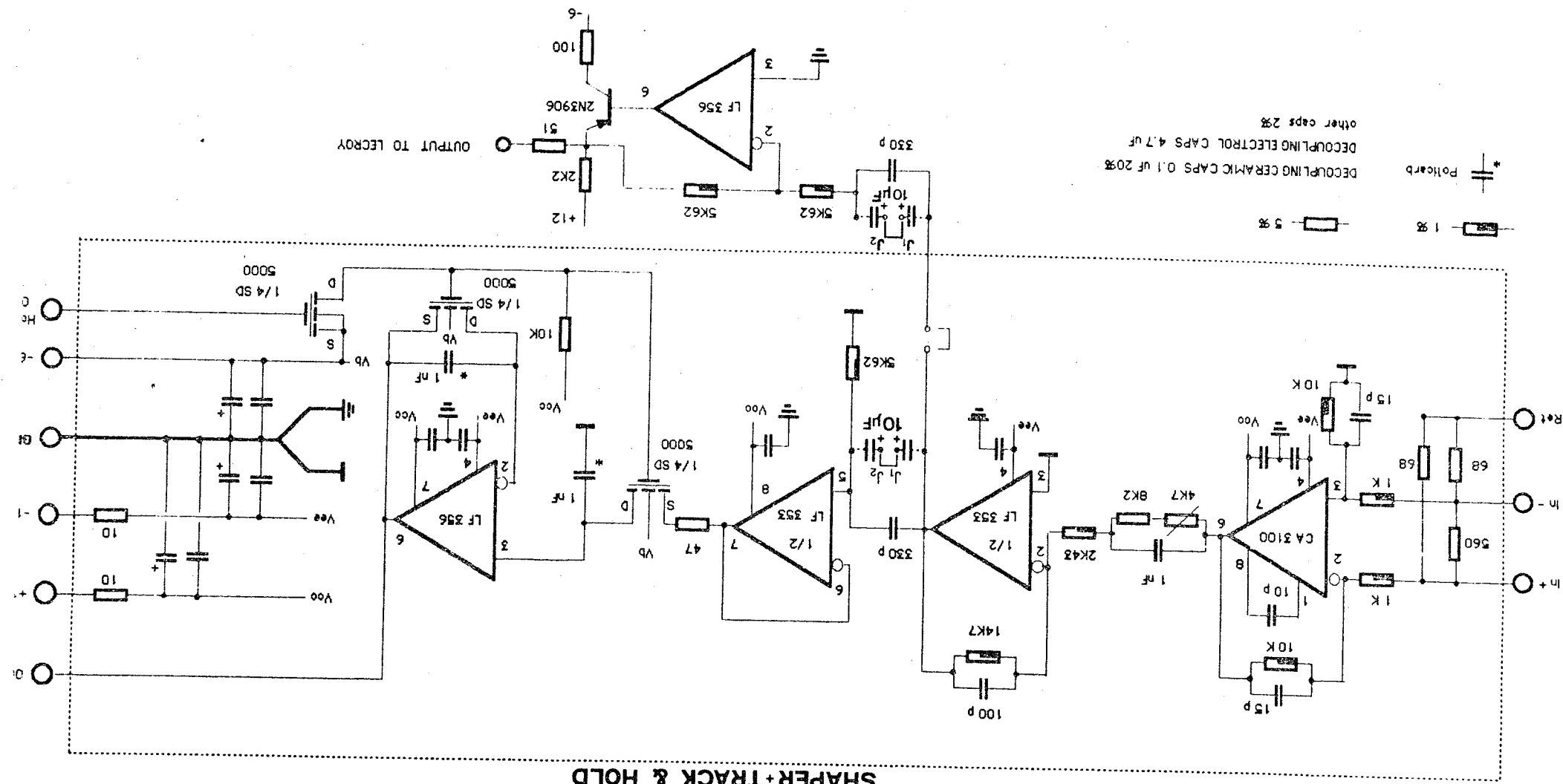


fig 6b

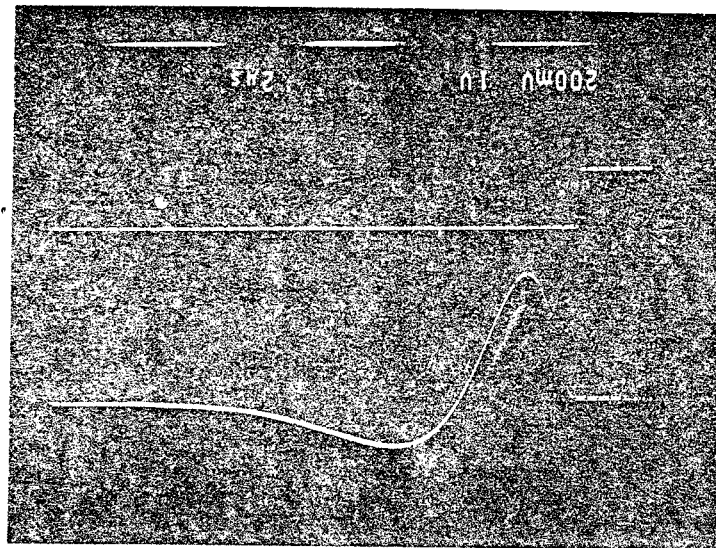


fig 6a

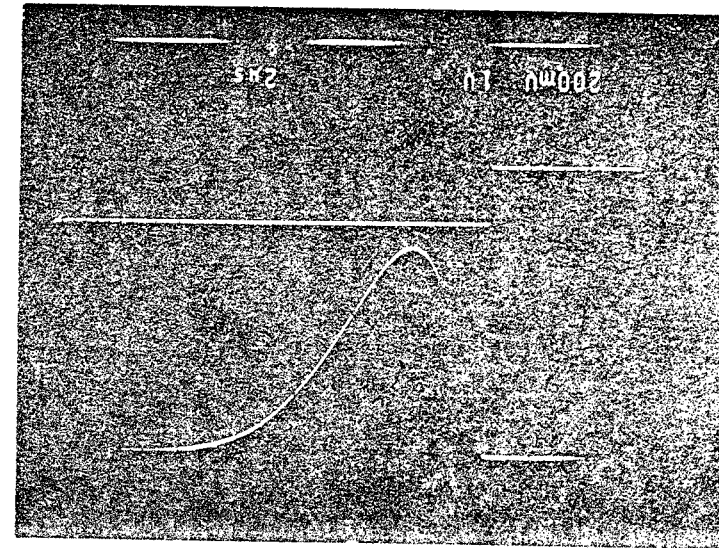


fig. 7

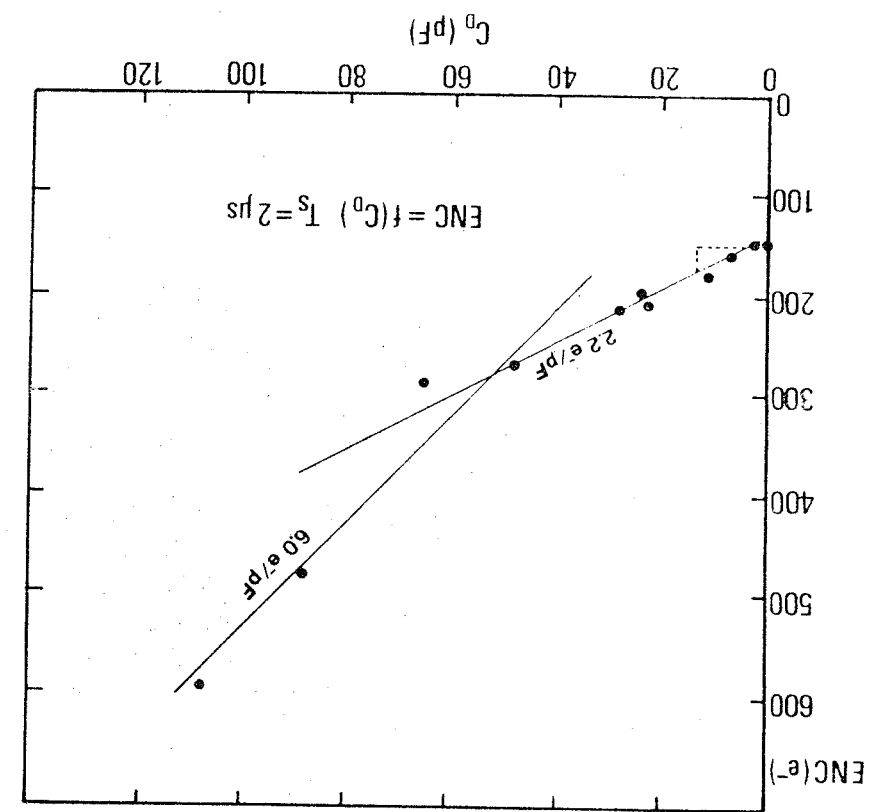


fig. 8

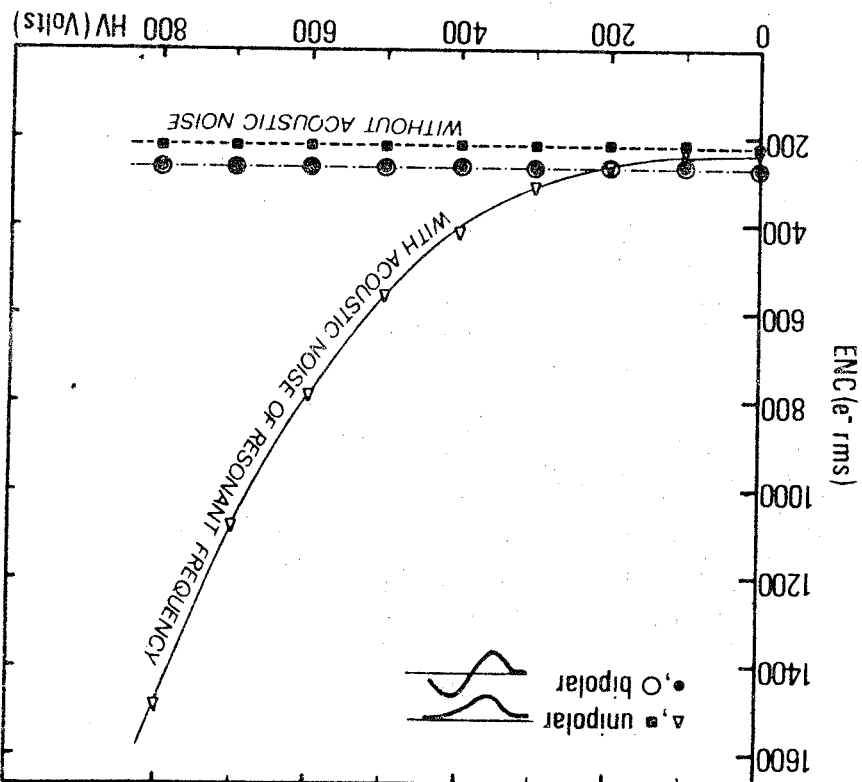


fig. 9

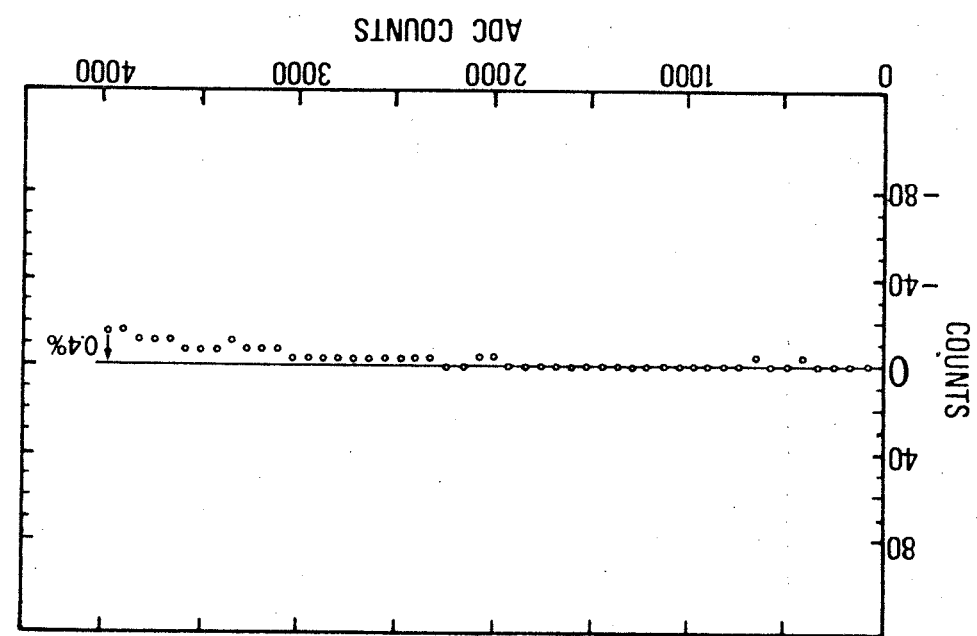


fig. 10

